ELSEVIER

Journal of Fluids and Structures 21 (2005) 151–167

JOURNAL OF FLUIDS AND STRUCTURES

www.elsevier.com/locate/jfs

Suppression of fluid force on a square cylinder by flow control

L. Zhou[a,*], M. Cheng[b], K.C. Hung[b]

[a]*Department of Naval Architecture, Dalian University of Technology, Dalian 116024, China*
[b]*Institute of High Performance Computing, 1 Science Park Road #01-01 The Capricorn Singapore Science Park II, Singapore 117528 Singapore*

Received 2 December 2003; accepted 16 July 2005

Abstract

A numerical study on reduction of fluid forces acting on a square cylinder (prism) in a two-dimensional channel using a control plate is presented in this paper. In order to control the flow around the square cylinder, a control plate is placed upstream. Fluid forces acting on the square cylinder, vortex shedding frequency and flow patterns are systematically investigated for different heights and positions of the control plate. The control plate height is varied from 10% to 100% of the square side width. For each height, the perpendicular distance between the control plate and the cylinder is varied from 0.5 to 3.0 times of the square width. The Reynolds number considered is 250, based on the square width, and the maximum incoming flow velocity. The technique used for the numerical analysis is the lattice Boltzmann method. Numerical studies show that not only is the drag on the square cylinder significantly reduced by the control plate, but also the fluctuating lift is suppressed as well. The optimum position of the control plate for minimizing the drag on the square cylinder is found for each control plate height.
© 2005 Elsevier Ltd. All rights reserved.

1. Introduction

Any body moving in a fluid experiences fluid forces. Among them, the resistance has been the major concern, since it directly relates to the energy required to move the body in the fluid. How to reduce the resistance (and thus save energy) remains a big challenge for mechanical engineers.

Besides resistance, the fluctuating lift is another concern. When a body is moving at a large Reynolds number, the vortex shedding behind the body becomes oscillatory, resulting in fluctuating forces acting on the body. Among them, the vertical fluctuating force, i.e. the fluctuating lift, induces the vertical vibration of the body. It is 1 of the main mechanisms that cause flow-induced vibration.

Flow control aims to reduce the resistance and the magnitude of the fluctuating force acting on the body. An effective flow control may save energy, increase propulsion efficiency and also reduce the vibration of the body.

A variety of ways have been designed to achieve better flow control. Among these methods, the approach to put a small bluff body in front of a big body is reportedly able to effectively suppress the fluid forces. This idea comes from the experimental studies by Morel and Bohn (1980), Igarashi (1982) and Koenig and Roshko (1985). Their experiments show that placing 2 bluff bodies in series in a uniform stream may sometimes lead to a total drag reduction compared to

*Corresponding author.
E-mail address: zhouli@dlut.edu.cn (L. Zhou).

0889-9746/$ - see front matter © 2005 Elsevier Ltd. All rights reserved.
doi:10.1016/j.jfluidstructs.2005.07.002

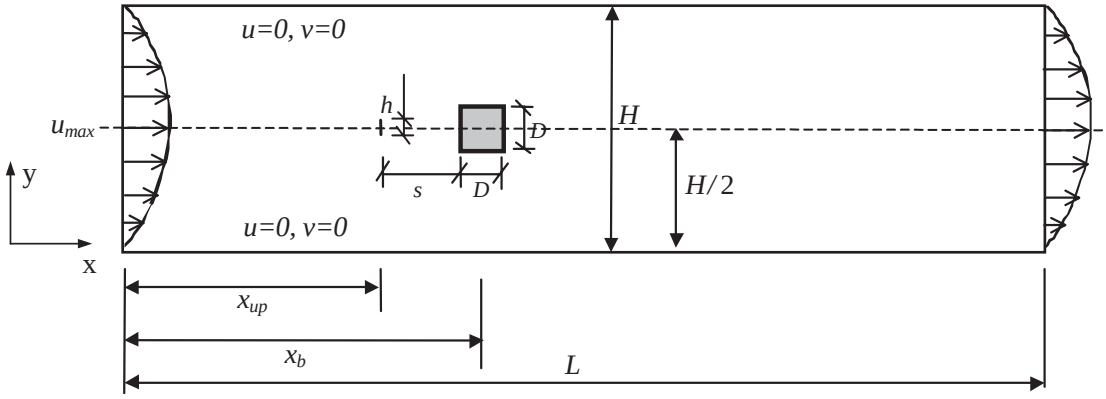

Fig. 1. Schematic of simulation model.

that of either body alone. Using this idea, a number of methods to reduce the drag and the side force were developed. Lesage and Gartshore (1987) successfully suppressed both the time-averaged drag and fluctuating forces on a bluff body by putting a small rod upstream. In their experiments, they used a flat plate, a square or a circular cylinder as the bluff body. The idea of flow control by the control rod in the separated shear layer was proposed by Igarashi and Tsutsui (1989). They found that by inserting a small cylinder in the shear layer near the main cylinder, a forced reattachment of the separated shear layer from the cylinder was realized, and the drag of the main cylinder was decreased. This idea was copied by Sakamoto et al. (1991) soon after. Igarashi and Ito (1993) reported the idea of flow control by the control rod in the upstream of the square prism. Drag reduction of the square prism was investigated in their experimental studies. Igarashi (1997) again presented his study of drag reduction on a square prism by use of a control rod. He also gave the critical gap distance between the prism and the control rod, at which the vortex shedding from the prism disappeared. Sakamoto et al. (1997) performed further investigations on the flow past a square prism with control. They put a flat control plate upstream and reported that the control plate suppressed the flow forces acting on the square prism.

All these studies have confirmed the effectiveness of this type of flow control. However, they are all based on experiments. A literature search shows that there are few numerical studies on the flow around a controlled square cylinder. Compared with experimental studies, numerical simulations are both cost-effective and more informative.

The objective of this paper is to numerically study the suppression of fluid forces acting on a bluff body by the use of a control plate. A flat plate is placed upstream of the square cylinder in order to control the approach flow to the square cylinder. The control plate height is varied from 10% to 100% of the square width (D in Fig. 1). For each height, the perpendicular distance between the control plate and the cylinder ranged from 0.5 to 3.0 times of the square width. The Reynolds number considered is 250, based on the square width and the maximum incoming flow velocity. The drag acting on the square cylinder and the whole system (square cylinder together with the control plate) as well as the fluctuating lift on the square cylinder are studied. In addition, the mechanism of reduction of the hydrodynamic loading around the square cylinder and the control plate are discussed, based on the visualized flow patterns.

We carefully compared various numerical methods used for solving Navier–Stokes (N–S) equations. We employ the lattice Boltzmann Method (LBM) because it is easy to implement and gives fast convergence. Conventional Computational Fluid Dynamics (CFD) methods start with discretizing the macroscopic N-S equations. But LBM is based on microscopic models and mesoscopic kinetic equations (Chen and Doolen, 1998). In LBM, the fluid field is discretized by a group of microscopic particles. The density distributions of these particles perform 2 types of motions: collision and streaming. The motions are governed by the Boltzmann Transfer equation in statistical mechanics. It is provable that the N–S equations can be derived from the Boltzmann Transfer equation by multi-scale analysis. The numerical implementation of LBM and the treatment of boundary conditions are easy. From published work (Chen and Doolen, 1998; Breuer et al., 2000) we can see that the simulation results using LBM agree well with other traditional method. Another feature of this method is that it is very well suited for parallel computing. Thus, the interest in LBM is fast increasing. The interested reader is referred to the review paper by Chen and Doolen (1998) and the excellent book by Wolf-Gladrow (2000).

2. Problem statement

Consider a two-dimensional square body in a channel, as shown in Fig. 1. The width of each side of the square is D. Throughout the paper, the dimension of the channel is represented by a length L and a width H. The centre of the square is positioned on the centre-line with coordinate at $(x_b, H/2)$. A control plate of height h is placed in front of the square cylinder. The distance from the frontal surface of the square cylinder to the control plate is s. Inlet and outlet boundaries are located at the left and right ends, respectively. The remaining boundaries are no-slip wall boundaries. The details of the boundary conditions will be discussed in Section 4.1.

Using (u, v) to denote the macroscopic velocities, the governing equations for the incompressible fluid flow are

momentum conservation

$$\frac{\partial \boldsymbol{u}}{\partial t} + (\boldsymbol{u}\nabla)\boldsymbol{u} = -\frac{1}{\rho}\nabla p(x, y; t) + \nu\nabla^2\boldsymbol{u}, \tag{1}$$

and *continuity*

$$\nabla \cdot \boldsymbol{u} = 0, \tag{2}$$

subject to suitable boundary conditions. Here $p(x, y; t)$ defines the pressure field; ν is kinematic viscosity. The nabla operator is $\nabla = (\partial/\partial x, \partial/\partial y)$.

The drag coefficient C_d, lift coefficient C_L and pressure coefficient C_p are defined by

$$C_d = \frac{F_D}{0.5\rho_0 u_{\max}^2 D}, \tag{3}$$

$$C_L = \frac{F_L}{0.5\rho_0 u_{\max}^2 D}, \tag{4}$$

$$C_P = \frac{(p - p_0)}{0.5\rho_0 u_{\max}^2}, \tag{5}$$

where F_D and F_L are resistance and lift respectively, ρ_0 is initial fluid density, $u_{\max}$ is the maximum velocity at the inlet, and p_0 is a reference pressure. The resistance coefficient of the total system is similarly defined by

$$C_{DT} = \frac{F_D + F_{D,\mathrm{pl}}}{0.5\rho_0 u_{\max}^2 D}, \tag{6}$$

where $F_{D,\mathrm{pl}}$ is the drag on the control plate.

Other nondimensional parameters to be used are the Reynolds number Re, nondimensional time t', Strouhal number St. They are defined by the following equations:

$$\mathrm{Re} = \frac{u_{\max} D}{\nu}, \tag{7}$$

$$t' = \frac{t u_{\max}}{D/2}, \tag{8}$$

$$\mathrm{St} = \frac{fD}{u_{\max}}, \tag{9}$$

where f is the frequency of vortex shedding.

3. Solution using of LBM

We now turn to solving the N–S Eqs. (1) and (2). As mentioned in the introduction, the LBM can solve the N–S equation indirectly. In LBM, the particle density distributions are stored on the lattice nodes. At every time step, the density distributions of the particles either "move" from 1 node to the other, or "remain" at the original position. In the present study we consider a two-dimensional square lattice with 9 velocities D2Q9 model shown in Fig. 2. These 9

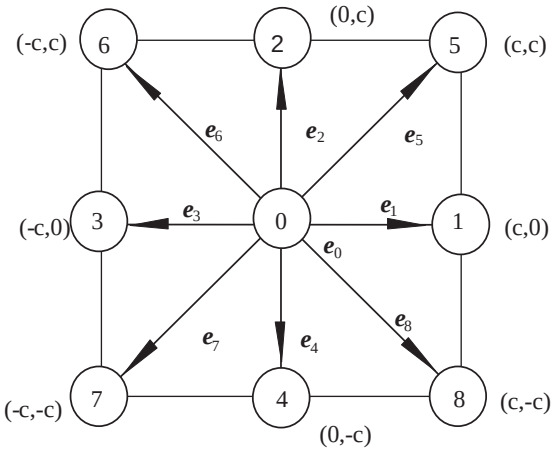

Fig. 2. LBM lattice velocities.

motion directions are denoted as $\mathbf{e}_\alpha(\alpha = 0, 1, ..., 8)$. The velocities $\mathbf{c}_\alpha$ at each node are then given by

$$\mathbf{c}_\alpha = c\mathbf{e}_\alpha = \begin{cases} (0,0), & \alpha = 0 \\ c\left[\cos\left(\frac{\alpha-1}{2}\pi\right),\ \sin\left(\frac{\alpha-1}{2}\pi\right)\right], & \alpha = 1,2,3,4 \\ \sqrt{2}c\left[\cos\left(\frac{\alpha-5}{2}\pi+\frac{\pi}{4}\right),\ \sin\left(\frac{\alpha-5}{2}\pi+\frac{\pi}{4}\right)\right], & \alpha = 5,6,7,8. \end{cases} \tag{10}$$

In the above equation, $c = \delta x/\delta t$, where δx and δt are the lattice separation and the time step.

The lattice Boltzmann equation with BKG approximation can be written as

$$f_\alpha(\boldsymbol{x} + \boldsymbol{c}_\alpha\Delta t, t + \Delta t) - f_\alpha(\boldsymbol{x}, t) = -\frac{1}{\tau}(f_\alpha(\boldsymbol{x}, t) - f_\alpha^{\mathrm{eq}}(\boldsymbol{x}, t)), \quad \alpha = 0, 1, 2, \ldots, 8, \tag{11}$$

where f_α is the single particle mass distribution function in the α direction, t is the time, Δt and $c_\alpha\Delta t$ the time and space increment, respectively; τ is the relaxation time due to collision. f_α^{eq} is the local equilibrium distribution function, which can be given as

$$f_\alpha^{\mathrm{eq}} = \rho w_\alpha\left[1 + \frac{3}{c^2}\mathbf{c}_\alpha\cdot\mathbf{u} + \frac{9}{2c^4}(\mathbf{c}_\alpha\cdot\mathbf{u})^2 - \frac{3}{2c^2}\mathbf{u}\cdot\mathbf{u}\right], \quad \alpha = 0, 1, 2, ..., 8 \tag{12}$$

with $w_0 = 4/9$, $w_\alpha = 1/9(\alpha = 1, 2, 3, 4)$ and $w_\alpha = 1/36(\alpha = 5, 6, 7, 8)$.

The macroscopic mass density ρ and the velocity $\boldsymbol{u}$ are the summations of the distribution functions

$$\rho = \sum_{\alpha=0}^{8} f_\alpha, \quad \rho\boldsymbol{u} = \sum_{\alpha=0}^{8} \boldsymbol{c}_\alpha f_\alpha. \tag{13}$$

Using the Chapman–Enskog expansion, i.e. multi-scale analysis, it is mathematically provable that the LBM Eq. (11) can recover the N–S equation to the second order of accuracy (Chen and Doolen, 1998) if the pressure is defined by

$$p = \rho c^2/3 \tag{14}$$

and the kinematic viscosity is defined as

$$v = (\tau - 0.5)c^2\Delta t/3. \tag{15}$$

Eq. (11) is an algebraic equation. Given the distribution function f_α at time t, we can obtain an estimate of its value at the next time step, as implied by Eq. (11). With f_α known, all macroscopic quantities can be evaluated from Eqs. (13) and (14). In conventional CFD methods, we often need to solve a Poisson equation to find the pressure p. In LBM, however, solving Eq. (11) yields all the information we are interested in.

The basic algorithm consists of 2 processes: streaming and collision. In the sequence of streaming, particles move to the neighbor nodes according to the lattice velocities. During the process of collision, the relaxation rule secures the new equilibrium states of particles.

4. Numerical experiments and code validation

4.1. Set-up of numerical experiments

The problem under consideration is the flow around a square cylinder with a control plate placed upstream of the cylinder, as shown in Fig. 1. A channel with a blockage ratio $H/D = 8$ is selected for the computational domain. Finite inlet and outlet lengths are chosen to replace the infinite channel domain. It is usually difficult to give the exact values of the size of the computational domain so as to cancel the inlet and outlet boundary effects; but there are some rules and available data that one can follow.

It is well known that the forces acting on the bluff body and the flow patterns around it are influenced by the in-flow profile, in-flow length and out-flow length (Davis et al., 1984; Sohankar et al., 1996). These influences become negligibly small as the body is located far away from the inlet and outlet. The study conducted by Sohankar et al. (1996) shows that to minimize the influences of in-flow and out-flow length, the minimum values of upstream and downstream extent should be over $11D$ and $30D$, respectively. Here D is the side width of the square cylinder. In the present study, the in-flow length is set to $12D$ and the total length of the domain is set to $50D$.

A parabolic profile with the maximum velocity $u_{\max}$ is applied at the inlet, on the left end of Fig. 1, in order to simulate a fully developed laminar channel flow. The same velocity profile is imposed at the outlet, at the right end. The flow at outlet has little effect on the flow upstream when the outlet is set far enough downstream of the cylinder (out-flow length $\geqslant 30D$). No-slip wall boundary conditions are applied to the remaining boundaries, including the surfaces of the square and the control plate, as well as the top and bottom boundaries of the channel, where a bounce-back boundary treatment is used. Initially the velocities at all nodes, except the nodes at inlet and outlet are set to zero, and an initial pressure $p_{\text{ini}} = 0.2/3$ is imposed at all nodes. In order to make the flow asymmetric initially, a small disturbance of velocity is applied to a particular point (not at the centreline) at the beginning; after several time steps, this disturbance is cancelled.

Another important factor to be considered before any numerical experiment is mesh density. The mesh density determines the accuracy of the results. We conducted some preliminary studies on mesh density. The parametric studies lead to the conclusion that 40 elements applied on each side of the square cylinder of width D are good enough to accurately calculate the hydrodynamic parameters and to capture the details of the flow patterns. In total 2000×320 elements are used.

4.2. Code validation

The code is validated against the problem of flow past a square cylinder without control in the range of $10 \leqslant \text{Re} \leqslant 250$. The results are compared with those presented by Breuer et al. (2000). Two parameters are validated: time-averaged drag coefficient and Strouhal number.

Time-averaged drag coefficient. One of the most important parameters for flow around an obstacle is the drag coefficient C_d. Fig. 3 shows the time-averaged drag coefficient C_d defined in Eq. (3) against Reynolds number. The solid line represents the results obtained from LBM, and the points denote results obtained by the finite volume method (FVM) (Breuer et al., 2000). The figure shows that the results obtained by LBM are in generally good agreement with those obtained by FVM. In the region of small Reynolds numbers ($\text{Re} \leqslant 60$), the drag coefficient varies strongly with Re. As the Reynolds number becomes larger ($\text{Re} > 60$), the drag coefficient varies mildly with Re. However, a discrepancy occurs at low Reynolds number ($\text{Re} = 10$). The reasons for this discrepancy may lie in the mesh densities and the mechanism of the drag components. 40 elements are used along each side of width D in the present study, while 100 elements were used in Breuer's study. When Re is small, the viscous component and the pressure force contribute to the total drag in the same order of magnitude. In that case, 40 elements on each side of the square cylinder are sufficient to obtain the pressure force, but a finer resolution is needed to capture the component of drag caused by viscosity. However, when Re is large, the dominant component is the pressure force, which accounts for more than 95% of the total drag. In this case, our mesh density is good enough to compute the drag.

Strouhal number. The Strouhal number defined in Eq. (9) is another important parameter, determining the shedding frequency of the Kármán vortex street in the wake. The characteristic frequency f is determined by a spectral analysis of time series of the lift coefficient. The computed Strouhal number is also compared with the Breuer et al. (2000) result as shown in Fig. 4, where LBM results are represented by a solid line with triangles, and the FVM results are illustrated by the diamond-points. It can be seen that the results of both methods agree well. At relatively low Reynolds number, $\text{Re} < 150$, Strouhal number increases with increasing Reynolds number. At relatively high Reynolds number, $\text{Re} > 150$,

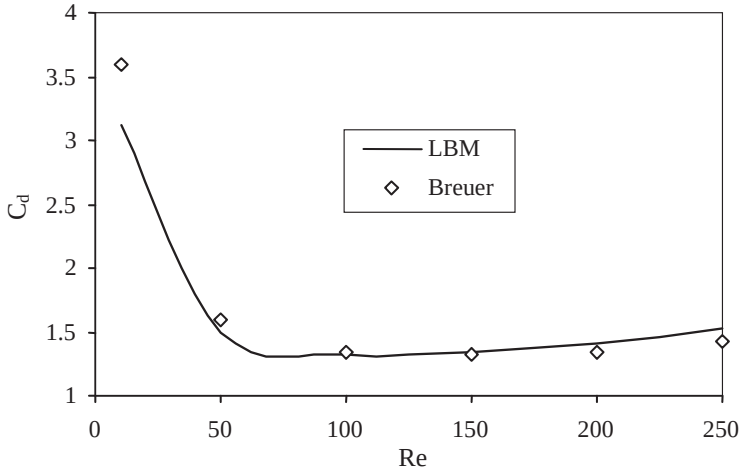

Fig. 3. Comparison with previous work for the drag coefficient.

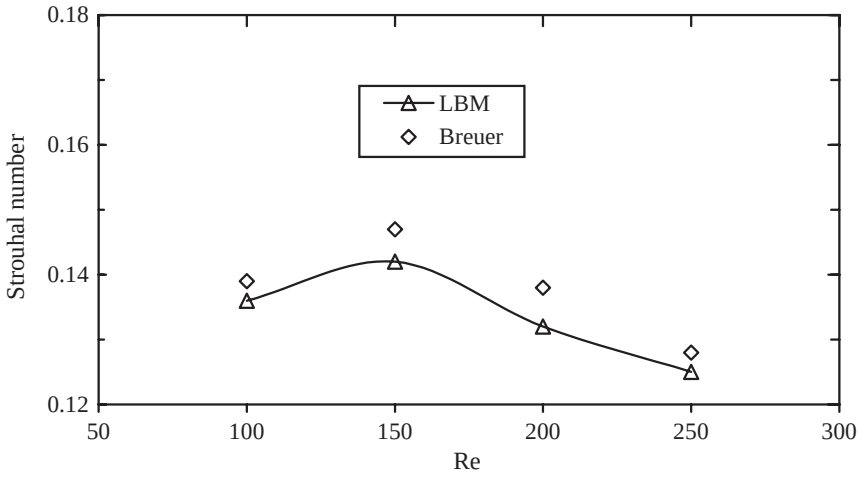

Fig. 4. Comparison with previous work for the Strouhal number.

Strouhal number decreases with increasing Reynolds number. The error $((St_{,FVM}-St_{LBM})/St_{LBM})$ is about 2.21%, 3.52%, 4.55% and 2.40% for Re of 100, 150, 200 and 250, respectively.

This result is also used as the baseline for the comparison between the flow around a square cylinder with control and without control. Flow around a square cylinder was also studied by Davis et al. (1982, 1984), Sohankar et al. (1996), Bernsdorf et al. (1998) and Cheng and Liu (2000).

5. Results and discussion

In this section, the effect of the control plate on the hydrodynamic parameters such as typical flow patterns, pressure distribution and the drag on the cylinder are discussed.

5.1. Typical flow patterns

Firstly, the control plate height is fixed, while its position is changed in order to investigate the effect of the position on the flow control. Typical flow patterns in vorticity contour plots for different control plate positions are shown in

Fig. 5. The corresponding variation of fluctuating lift against time and the corresponding spectra are given in Fig. 6. Secondly, the control plate height is varied with the position unchanged to investigate the effect of the height on the flow. Typical flow patterns described by the vorticity contour versus control plate height are shown in Fig. 7. The related fluctuating lift and its spectrum analysis are plotted in Fig. 8. The time selected for the flow patterns is at a nondimensional time of $t' = 250$.

From Fig. 5, an alternating Kármán vortex street is observed in the wake region downstream of the square cylinder. However, compared to the flow without control (Fig. 5(a)), the width of the wake downstream of the square cylinder is narrow when the control plate is used (Figs. 5(b)–(e)). The number of the vortices shed behind the square cylinder is also different: there are 6 vortices within the considered wake region of the square cylinder without control (Fig. 5(a)), while 7 or 8 vortices appear in the region downstream of the square cylinder with control (Figs. 5(b)–(e)). Another notable phenomenon is that the incoming flow to the square cylinder is entirely different when the control plate is utilized. The front surface of the cylinder is exposed to the wake region formed by the control plate. When the spacing between the 2 bodies is not too large, for example, $s/D = 0.5$, 1.0 or 2.5 (Figs. 5(b)–(d)), there are 2 stationary vortices between the 2 bodies. The size of the vortices between the 2 bodies is increased as the spacing is increased. When $s/D = 2.5$ (Fig. 5(d)), the size of the vortices reaches a maximum value. Moreover, the width of the vortex street behind the square cylinder is also the narrowest among the 5 cases. This illustrates that the control plate achieves its best effect for such a position. If the spacing is increased to $s/D = 3.0$ (Fig. 5(e)), the flow pattern is qualitatively changed. Besides the Kármán vortex street in the wake of the square cylinder, obviously alternate vortex shedding also occurs behind the control plate. This is due to the fact that the Reynolds number of the control plate is 75 for such a plate height (the critical Reynolds number of a flat plate with the present domain configuration is 40), and the behavior of the control plate becomes independent due to the relative large spacing. Therefore, it is not strange that a Kármán vortex street forms behind both the control plate and the square cylinder.

Fig. 6 shows the lift coefficient of the square cylinder defined in Eq. (4) against time and the corresponding spectra for various positions of the control plate. The lift acting on the square cylinder is consistent with the flow pattern around the cylinder. The near-sinusoidal variation of the lift curve indicates the periodic nature of vortex shedding from the cylinder. The negative peaks are caused by the shedding of vortices from the upper side of the cylinder, and vice versa. Compared to the lift on the square cylinder without control (Fig. 6(a)), the fluctuating lift on the controlled cylinder is well suppressed (Figs. 6(b)–(e)). The amplitude of the fluctuating lift is about 1.0 when the flow is not controlled. When the control plate is placed upstream the cylinder at $s/D = 1.0$ (Fig. 6(c)), the amplitude of the lift is about 0.25. The amplitude is further decreased to about 0.15 if the spacing is increased to $s/D = 2.5$ (Fig. 6(d)). However, the lift amplitude rebounds upwards if the spacing is kept increasing (Fig. 6(e)), because the interaction between the bodies becomes weaker.

Besides the amplitude of the lift, the spectra of the lift also change, which indicates that the frequency of the vortex shedding downstream of the square cylinder is changed. It is found that the vortex shedding frequency generally becomes high if the control plate is used. For example, the peak value of the frequency spectrum is around 0.063 Hz, corresponding to a Strouhal number of 0.126 for the flow without control, whereas the peak value is around 0.096 Hz, corresponding to a Strouhal number of 0.192 when $s/D = 1.0$ with $h/D = 0.3$. The vortex-shedding frequency is also changed with position of the control plate. The oscillation exhibits a single frequency if the flow is without control (Fig. 6(a)) or the control plate is near to the cylinder (Figs. 6(b) and (c)). When the control plate is used at $s/D = 2.5$ (Fig. 6(d)), there are 2 prominent frequencies in the lift spectrum. As the spacing is further increased to 3.0 (Fig. 6(e)), the 2 dominant frequencies of the lift spectrum are more notable, and the lift coefficient becomes irregular. The waveform of the lift signal arises from the complex interaction of the 2 rivaling frequencies. The multi-frequency characteristic is due to the 2 Kármán vortex streets, from both the square cylinder and the control plate.

Fig. 7 shows the vorticity contours of the flow controlled by a plate positioned at $s/D = 3.0$ with various heights. When h/D is from 0.1 to 0.7 (Figs. 7(a)–(f)), alternate vortex shedding behind the square cylinder is observed. The width of the Kármán vortex street becomes gradually narrower as the control plate height increases. When $h/D = 0.8$ (Fig. 7(g)), the vortex shedding becomes very weak. Increasing the control plate height further to $h/D = 0.9$ (Fig. 7(h)), the alternating vortex shedding disappears in the wake of the cylinder, and the flow is almost steady. This indicates that the vortex shedding behind the square cylinder is effectively suppressed if the control plate is placed at a suitable position with proper height. Vortex shedding behind the square cylinder is observed again when the control plate height is $h/D = 1.0$ (Fig. 7(i)).

Moreover, control plate height has direct influence on the wake downstream of the control plate. This results in a change of in-flow towards the square cylinder. It is well known that the flow pattern in the wake of a bluff body is related to the Reynolds number. When Re is low, no Kármán vortex street can be detected in the wake of the body. When Re is above a certain value, a Kármán vortex street is visible in the wake of the bluff body. The critical Reynolds number for a Kármán vortex street to be formed from a square cylinder is given as 70 and 54 by Okajima (1982) and

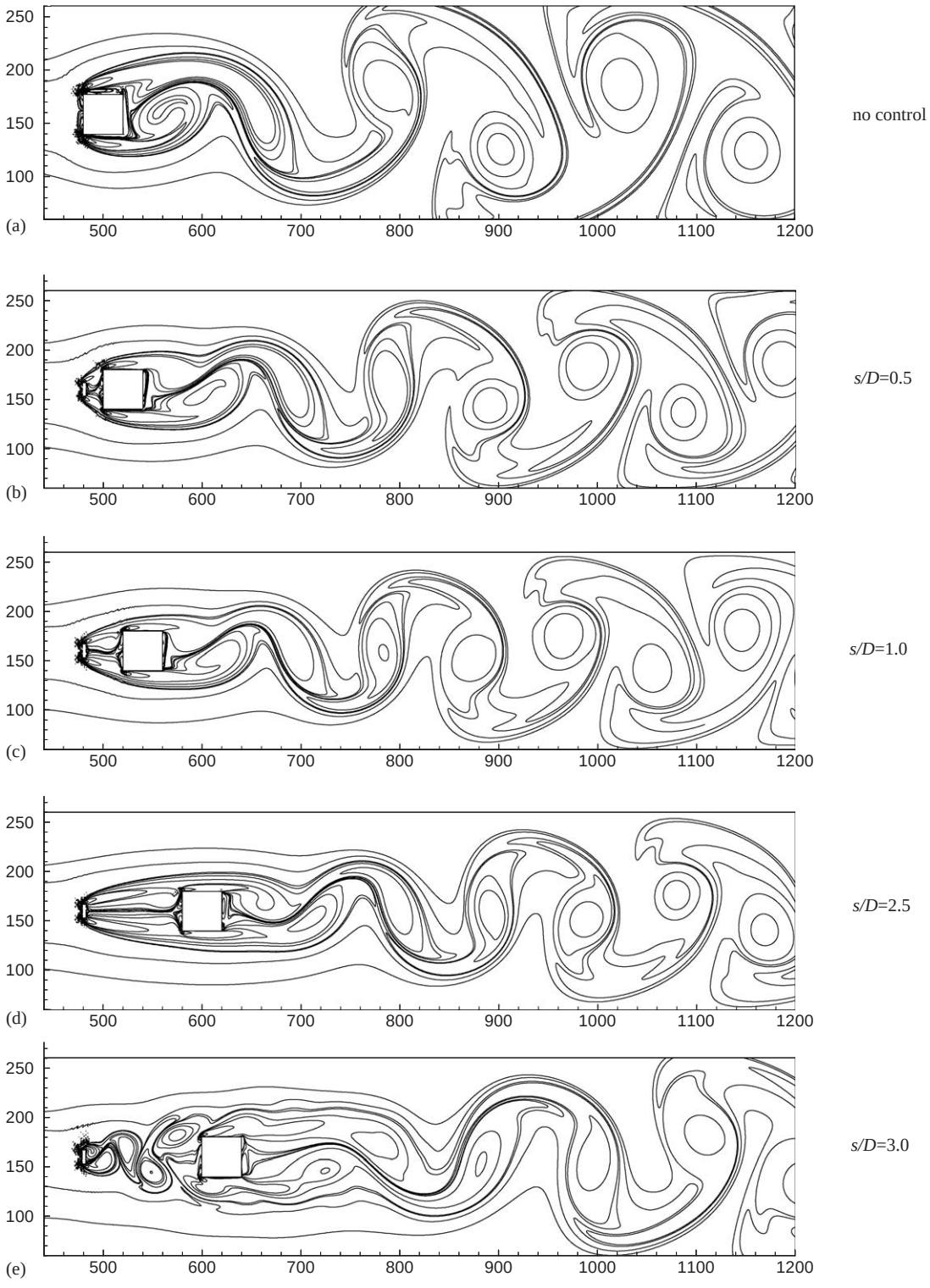

Fig. 5. Flow pattern with control plate of $h/D = 0.3$ at different positions.

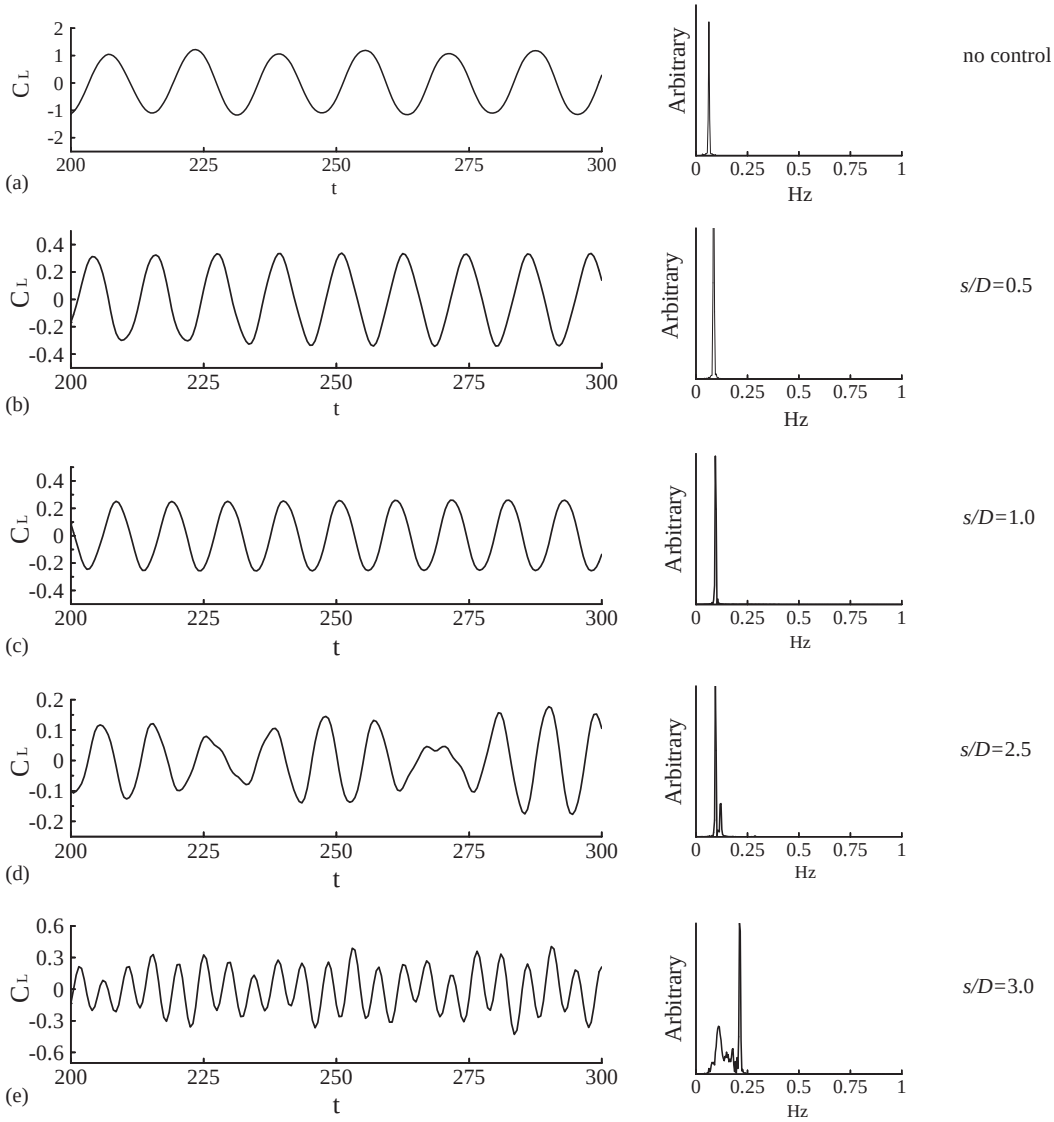

Fig. 6. Time histories of lift coefficient and power spectra of fluctuating lift $h/D = 0.3$.

Klekar and Patankar (1992), respectively. In the present study, it is found that the critical Reynolds number for a square cylinder is about 70, and the number for a flat plate is about 40. When $h/D = 0.1$ (Fig. 7(a)), the Reynolds number of the plate is 25, and there is no alternate vortex shedding behind the control plate. Instead, 2 small stationary vortices attached to the rear side of the plate are observed. When $h/D = 0.2$ and 0.3 (Figs. 7(b) and (c)), the Reynolds number of the plate is 50 and 75, respectively, and a Kármán vortex street is observed in the wake of the control plate. As the control plate height is further increased ($h/D = 0.5 \sim 1.0$ as shown in Figs. 7(d)–(i)), the flow behind the control plate again becomes stable, and 2 stationary vortices between the 2 bodies are found. The reason is that even though the Reynolds numbers are bigger than the critical number at such control plate heights, the limited space between the 2 bodies prevents the Kármán vortex street from forming.

Fig. 8 shows the waveform of the fluctuating lift of the square cylinder and the corresponding spectra for various control plate heights. Periodic variation of lift with a single frequency is found when $h/D = 0.1$, 0.5, 0.6 and 0.7 (Figs. 8(a),(d),(e) and (f)), respectively. For these cases, the Kármán vortex street is only observed in the wake of the square cylinder as shown in Figs. 7(a),(d),(e) and (f). Periodic lift fluctuation with multiple frequencies is found when $h/D = 0.2$ and 0.3 (Figs. 8(b) and (c)). For these 2 cases, alternate vortex shedding behind both the control plate and the

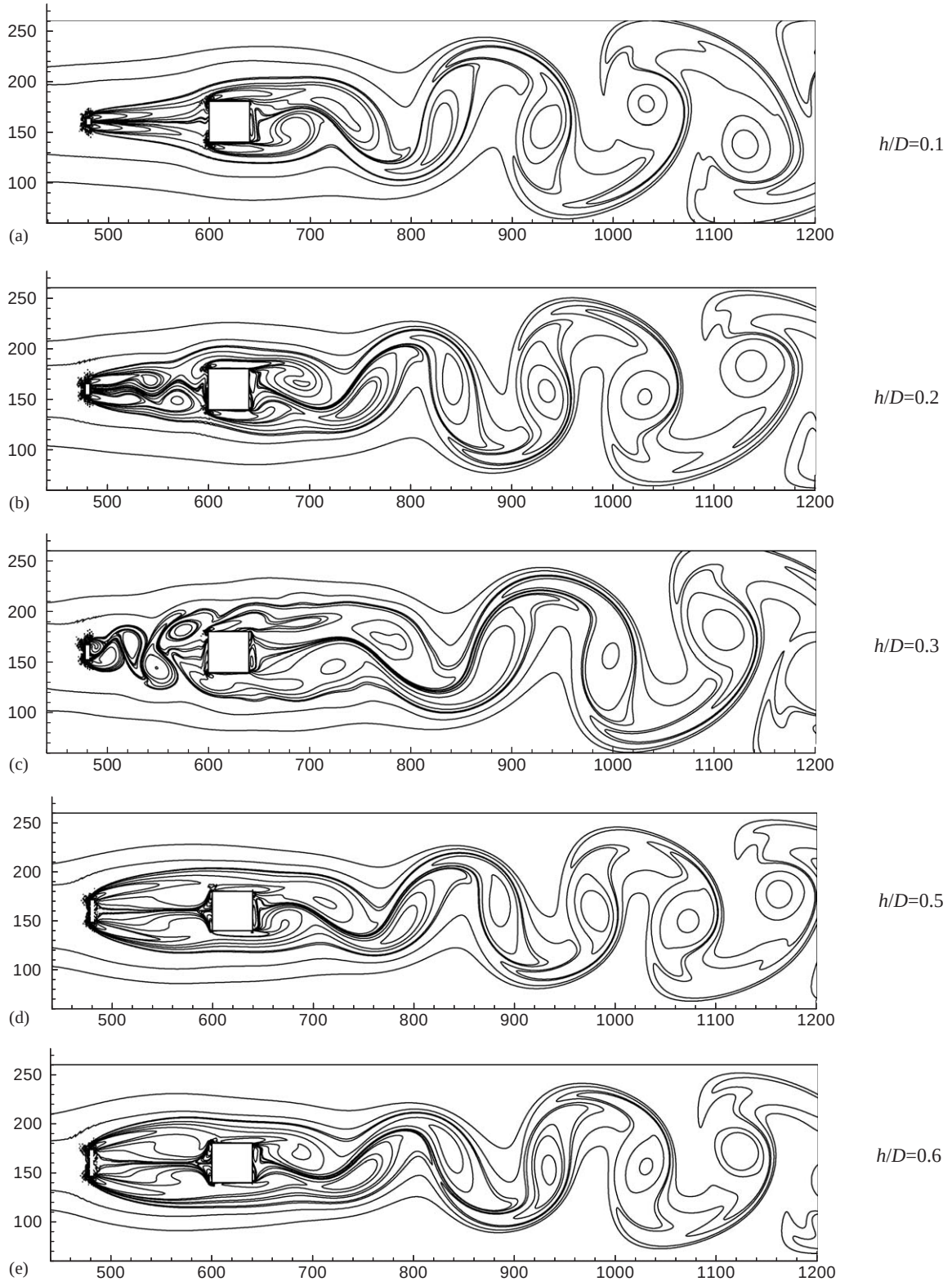

Fig. 7. Flow patterns for different control plate heights at position of $s/D = 3.0$.

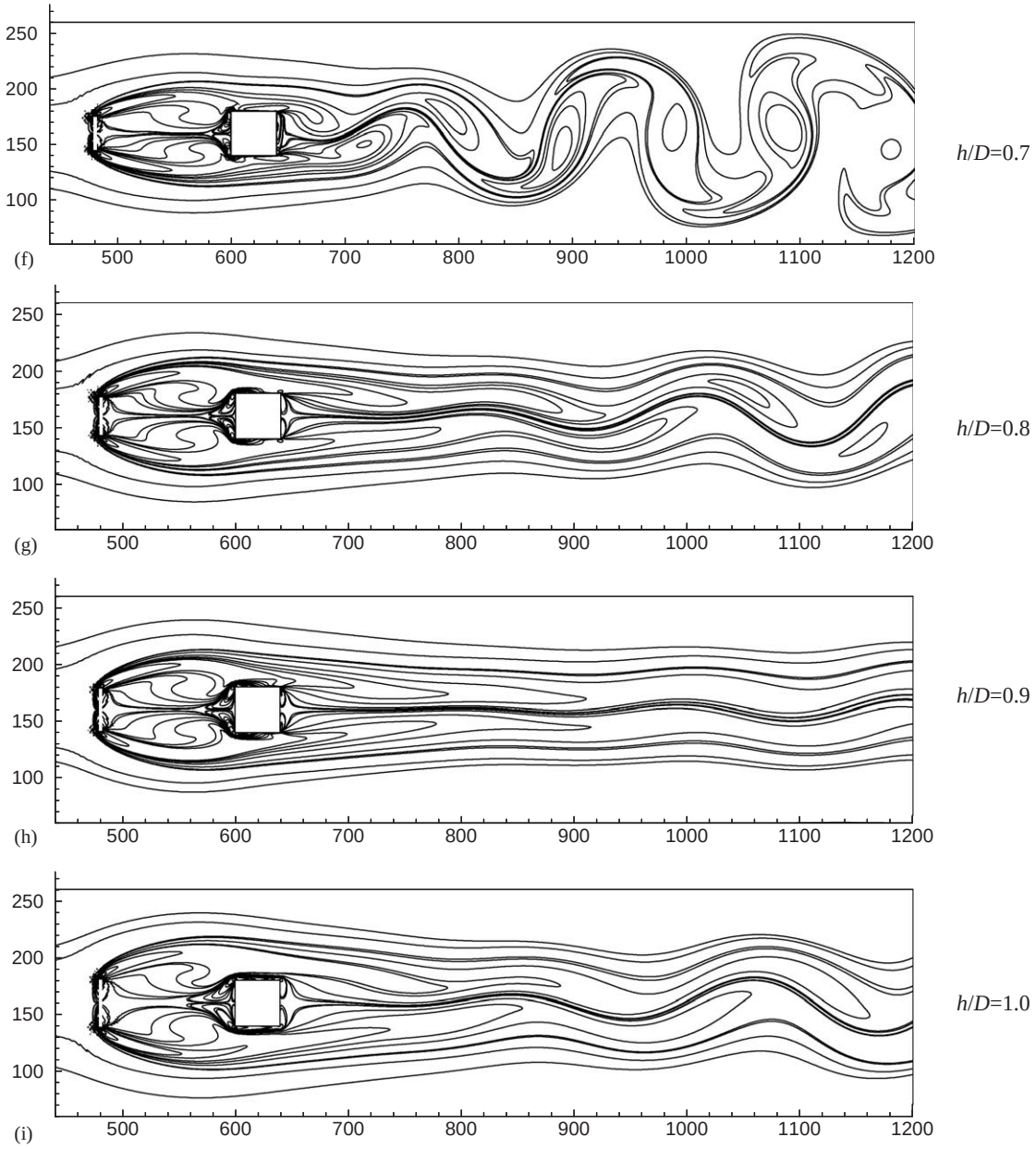

Fig. 7. (*Continued*)

square cylinder is observed, as shown in Figs. 7(b) and (c). The periodic lift fluctuation becomes very weak when $h/D = 0.8$ (Fig. 8(g)). When $h/D = 0.9$ (Fig. 8(h)), the value of the lift coefficient is almost a constant, and no distinct peak in the spectrum is observed. This is related to the stable wake flow (Fig. 7(h)). A slight periodic lift fluctuation is observed again when $h/D = 1.0$ (Fig. 8(i)).

5.2. Pressure distribution on the square cylinder

Fig. 9 shows the distribution of the time-averaged pressure coefficient C_p on the surface of the square cylinder for different control plate positions with $h/D = 0.3$. The solid line denotes the pressure coefficient when the square cylinder

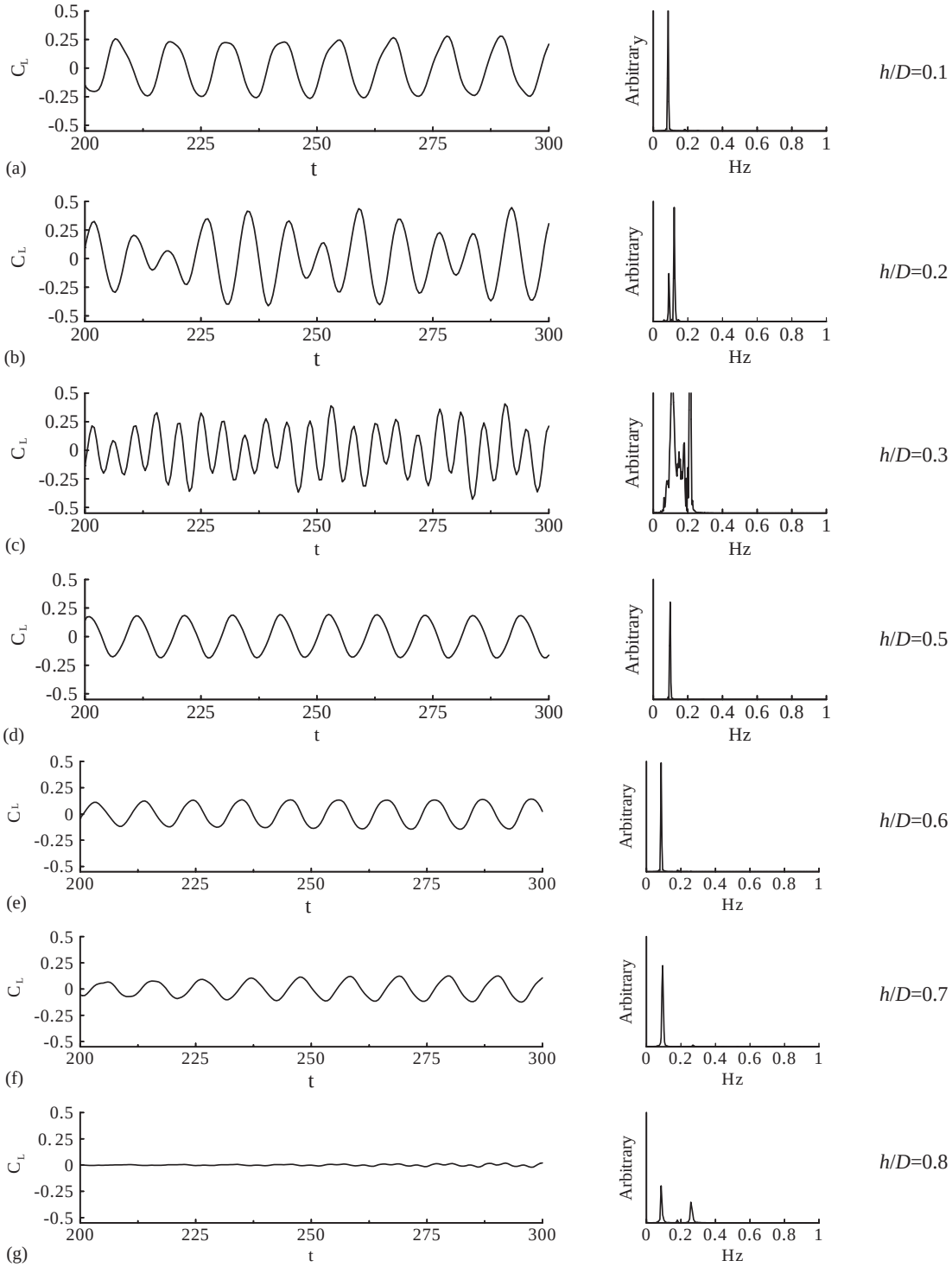

Fig. 8. Time histories of lift coefficient and power spectra of the fluctuating lift $s/D = 3.0$.

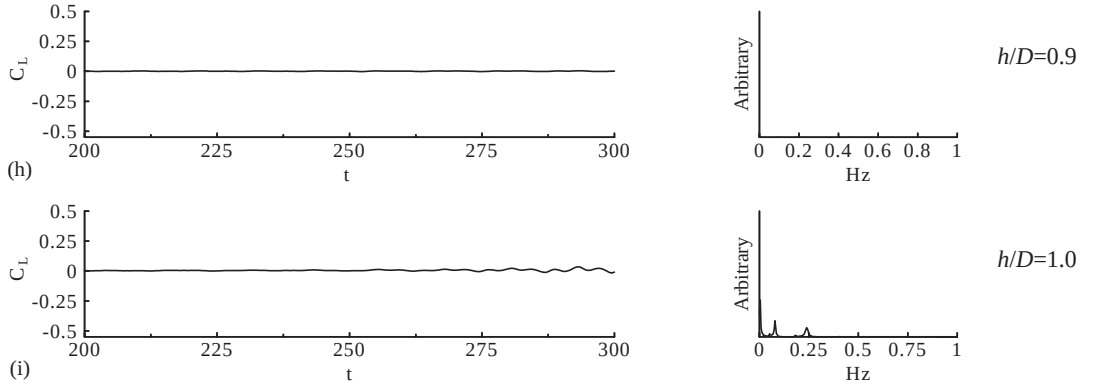

Fig. 8. (*Continued*)

is without control. The remaining lines represent the pressure coefficient on the cylinder when a control plate is used. The control plate is positioned at $s/D = 0.5$, 1.0, 2.5 and 3.0. It is found that, when a control plate is used, the variation of the time-averaged pressure coefficient is smaller than that without the control plate. On the front surface of the cylinder, the pressure is well suppressed by the control plate. When $s/D = 0.5$, 1.0 and 2.5, the pressure distribution is concave, and the pressure decreases with increasing spacing. When $s/D = 3.0$, the pressure distribution on the front surface of the square cylinder increases compared to that in other positions, and the curve becomes convex. Despite the increase in pressure (which is due to the Kármán vortex street forming behind the control plate), the pressure on the front surface of the cylinder is still smaller than that without the control plate. In addition, when a control plate is used, the time-averaged pressure coefficient on the rear surface of the square cylinder increases but its magnitude decreases (note that it is negative). The reason is that the alternate vortex shedding downstream of the square cylinder is suppressed by the control plate.

It is interesting to note that the experimental investigation on the same problem conducted by Sakamoto et al. (1997) gave similar results for the effect of a control plate. Although the Reynolds number of the present study ($Re = 250$) is different from that of the experimental investigation ($Re = 5.6 \times 10^4$), the pressure distribution on the square cylinder with a control plate in the experimental study demonstrated similar regularity as the present study. Similar pressure distribution was also observed in the experimental study conducted by Mahbub Alam et al. (2002) for a flow past 2 square prisms controlled by a flat plate. This is expected since the control plate placed upstream of the square cylinders play same role in the flow control.

5.3. Reduction of the drag and r.m.s. lift

In this section, the drag acting on the square cylinder and the control plate as well as the r.m.s. value of the lift on the cylinder are investigated. The drag and lift forces are directly relevant to the flow features around the 2 bodies.

Fig. 10 shows the relationship between the time-averaged drag coefficient C_d and the position of the control plate for different plate heights. The C_d value of the square cylinder without the control plate is about 1.529, which is shown in Fig. 10 with a dotted straight line. Drag acting on the cylinder obviously reduces when the control plate is used. The reduction is due to the change in the in-flow towards the square cylinder. When the control plate is placed upstream of the cylinder, the cylinder is in the wake region of the control plate. Low pressure in this wake region results in the reduction of the drag of the cylinder. In addition, the suppression of the Kármán vortex street downstream of the square cylinder leads to pressure increase in this region, thereby decreasing the drag.

The height of the control plate plays an important role in drag control. As the control plate height increases, the drag of the square cylinder normally decreases. As shown in Fig. 7, 2 small vortices attach to the control plate when $h/D = 0.1$; alternate vortex shedding occurs behind the control plate when $h/D = 0.2$ and 0.3; 2 large vortices stay between the 2 bodies when $h/D = 0.5 \sim 1.0$. This indicates that the pressure in front of the cylinder becomes lower and lower as the plate height increases. In addition, the suppression of alternate vortex shedding behind the square cylinder normally becomes better as the control plate height increases. Therefore, the drag on the cylinder decreases as the height increases. When the control plate is high enough, say $h/D \geqslant 0.6$, the drag on the square cylinder is negative. This indicates that the horizontal force acting on the cylinder has changed from a drag to a propulsive force instead.

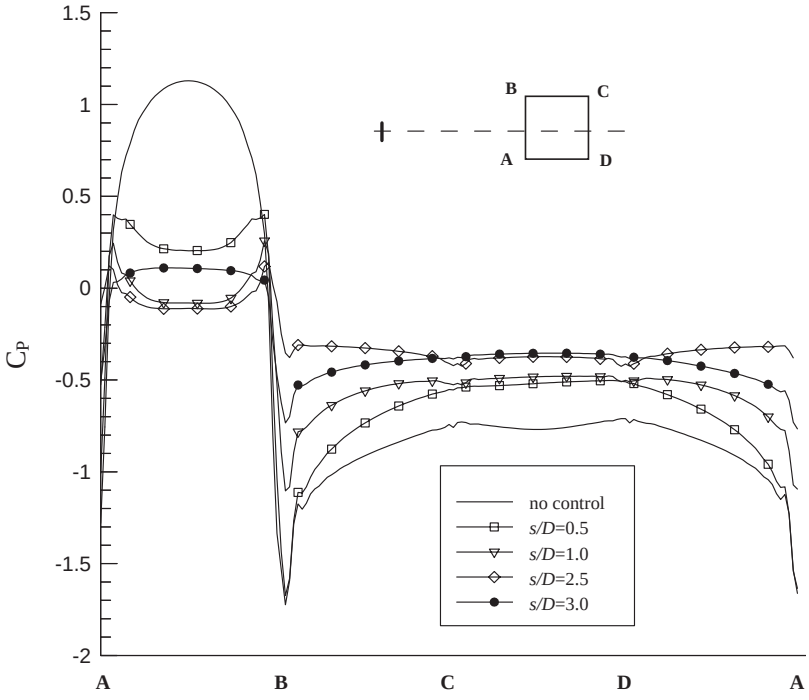

Fig. 9. Pressure coefficient on the surface of the square cylinder for different positions s/D with $h/D = 0.3$.

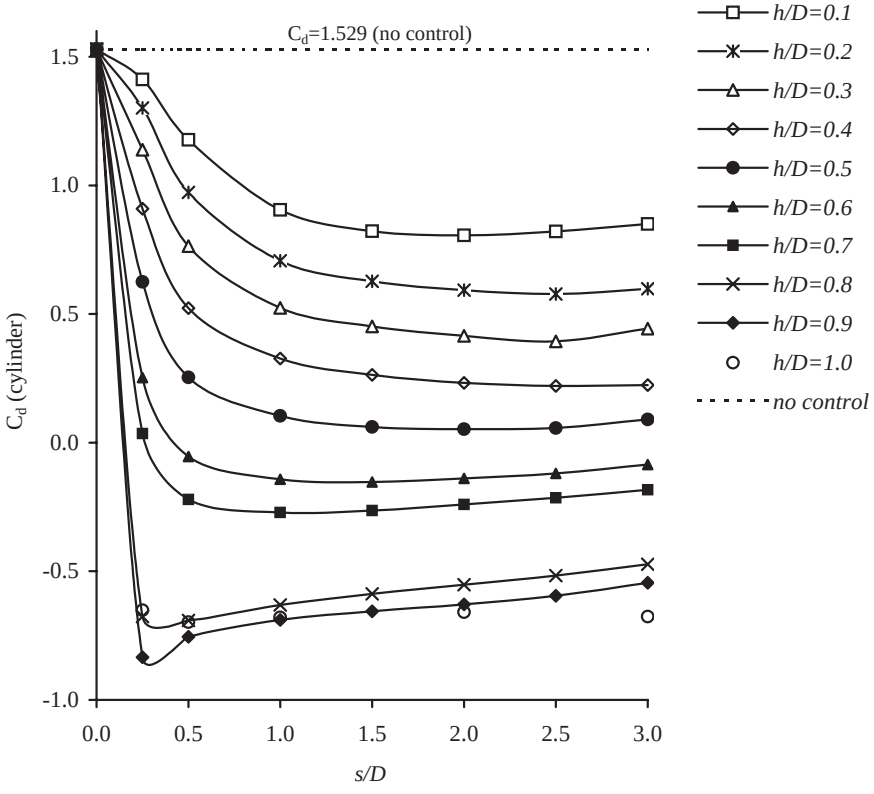

Fig. 10. Time-averaged drag coefficient of the square cylinder versus spacing s/D for various control plate heights h/D.

Table 1
Maximum drag reduction for different control plate heights

h/D	0.1	0.2	0.3	0.4	0.5	0.6	0.7	0.8	0.9	1.0
s/D	2.0	2.5	2.5	2.5	2.0	1.5	1.0	0.5	0.25	0.5
Maximum drag reduction	0.473	0.622	0.742	0.856	0.965	1.100	1.177	1.452	1.546	1.456

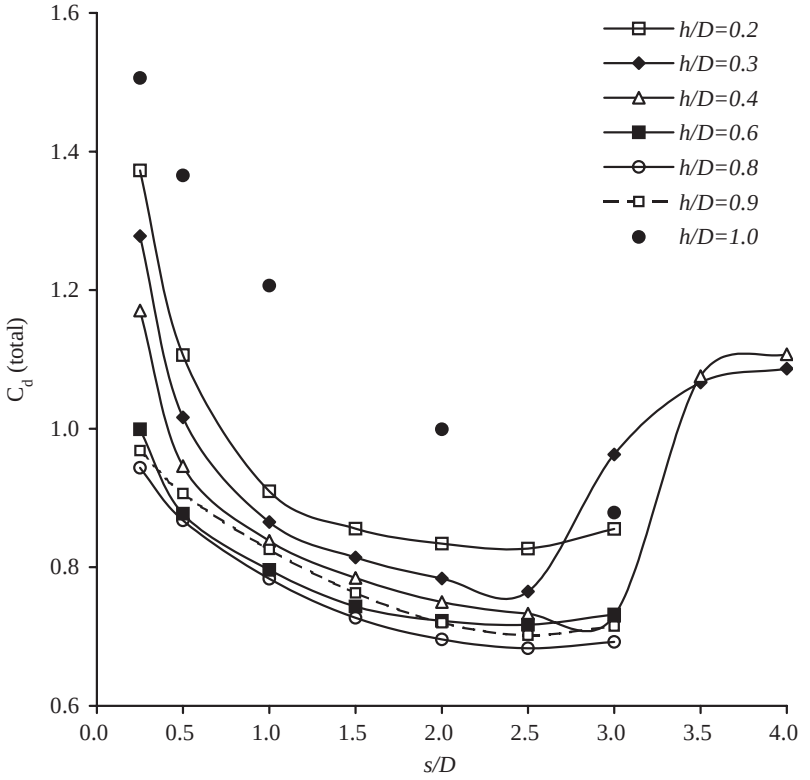

Fig. 11. Total drag coefficient versus spacing s/D for various control plate heights h/D.

Another important parameter for drag control is the spacing between the square cylinder and the control plate. For each plate height, the appropriate position corresponding to the minimum drag on the square cylinder is found. The optimum position as well as the maximum drag reduction value $(C_{d0} - C_d)/C_{d0}$, in which C_{d0} is the time-averaged drag coefficient of the square cylinder without the control plate, are shown in Table 1. The maximum reduction reaches approximately 74%, 96% and 145% for $s/D = 2.5$ with $h/D = 0.3$, $s/D = 2$ with $h/D = 0.5$, and $s/D = 0.5$ with $h/D = 1.0$, respectively.

Total drag, i.e. the sum of the drag acting on the square cylinder and the control plate is another concern in our study. Fig. 11 shows the total drag coefficient as a function of the control plate position for different plate heights. The figure shows that the total drag is generally a decreasing function of the control plate height. However, when the height reaches a certain level ($h/D = 0.9$, for the present study), the total drag begins to increase. When $h/D = 1.0$, the total drag increases significantly, although the drag on the square cylinder decreases. The increase of the total drag is due to the increase in drag induced by the plate.

One interesting feature found in the results is that at $s/D = 3.0$ with $h/D = 0.3$, the total drag increases significantly. This is due to the occurrence of the Kármán vortex street behind the control plate (as explained for Fig. 5(e)), which leads to considerable increase in the drag acting on the plate. In order to confirm this explanation, an additional case at $s/D = 3.5$ with $h/D = 0.4$ is studied. A similar phenomenon is observed, as expected. This phenomenon cannot be found if there is no Kármán vortex street downstream of the control plate. As the spacing further increases ($s/D = 3.5$ with $h/D = 0.3$; $s/D = 4.0$ with $h/D = 0.3$; and $s/D = 4.0$ with $h/D = 0.4$), the total drag coefficient increases slowly.

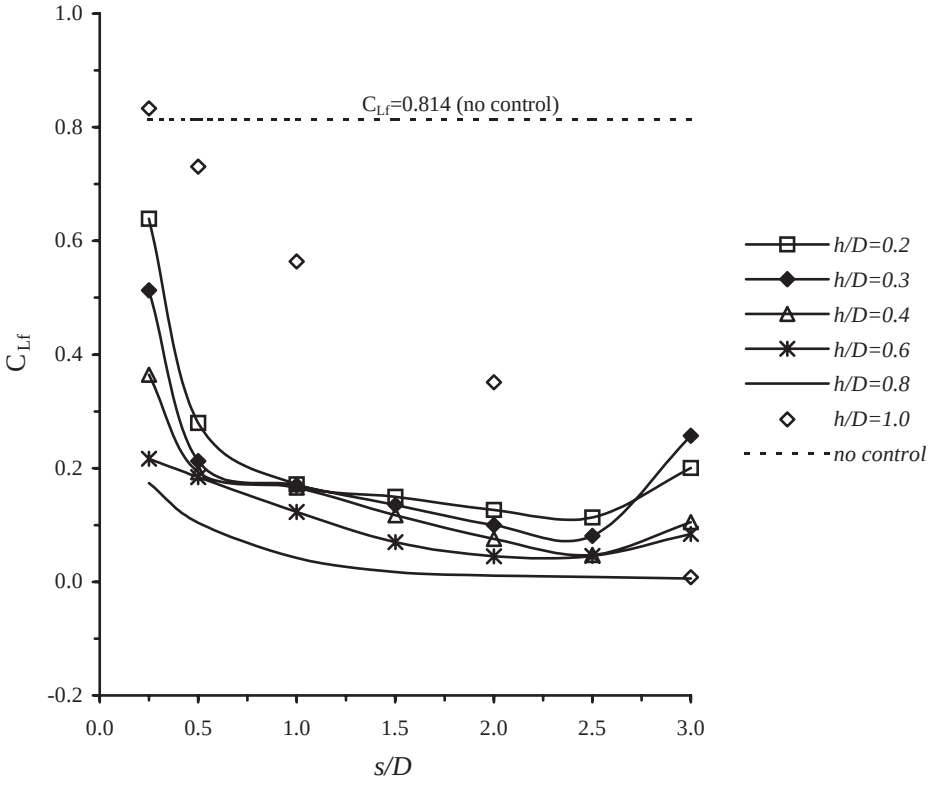

Fig. 12. R.m.s lift coefficient of square cylinder versus spacing s/D for different control plate heights h/D.

Fig. 12 shows the r.m.s. value of the lift coefficient on the square cylinder versus the position of the control plate for different control plate heights. The time-averaged lift is almost zero due to the structural symmetry. From these results, we can conclude that the amplitude of the fluctuating lift acting on the square cylinder is reduced by the control plate. Both position and height of the control plate have influences on the reduction. For each control plate height, the amplitude of the fluctuating lift decreases as the spacing increases till the spacing exceeds a certain value, at which obvious alternate vortex shedding occurs behind the control plate. Generally, for a particular spacing, the amplitude of the fluctuating lift decreases as the plate height increases. However, when the height reaches a certain value ($h/D = 1.0$), the amplitude of the fluctuating lift increases significantly compared to those for other control plate heights considered in the present study.

6. Conclusions

A numerical study on suppression of fluid forces on a square cylinder in cross-flow controlled by a flat plate has been conducted. The existence of the control plate changes the flow features in front of the square cylinder totally. The drag acting on the square cylinder and the total drag acting on the 2 bodies (the square cylinder together with the control plate) are normally reduced by the control plate. If a control plate is fixed at a position upstream of the cylinder, the drag on the square cylinder decreases as the control plate height increases. Negative drag on the square cylinder is achieved if the control plate is high enough. The maximum reduction of the drag acting on the square cylinder and the optimum position of the control plate are given for a particular control plate height. The total drag coefficient, i.e. the sum of the drag coefficient of the square cylinder and the control plate, are also generally reduced as the plate height increases. Although the drag on the square cylinder becomes smaller and smaller as h/D approaches 1.0, the total drag, nevertheless, increases significantly. The present study has also revealed that the amplitude of the fluctuating lift on the square cylinder is well suppressed if the control plate is used. The fluctuating lift can be completely suppressed if the control plate with a certain height is placed at an appropriate position.

References

Bernsdorf, J., Zeiser, T., Brenner, G., Durst, F., 1998. Simulation of a 2D channel flow around a square obstacle with lattice Boltzmann (BGK) automata. Journal of Modern Physics C 9, 1129–1141.

Breuer, M., Bernsdorf, J., Zeiser, T., Durst, F., 2000. Accurate computations of the laminar flow past a square cylinder based on two different methods: lattice Boltzmann and finite-volume. Journal of Heat and Fluid Flow 21, 186–196.

Chen, S.Y., Doolen, G.D., 1998. Lattice Boltzmann method for fluid flows. Annual Review of Fluid Mechanics 30, 329–364.

Cheng, M., Liu, G.R., 2000. Effect of afterbody shape on flow around prismatic cylinders. Journal of Wind Engineering and Industrial Aerodynamics 84, 181–196.

Davis, R.W., Moore, E.F., Purtell, L.P., 1984. A numerical–experimental study of confined flow around rectangular cylinders. Physics of Fluids 27, 46–59.

Igarashi, T., 1982. Characteristics of a flow around two circular cylinders of different diameters arranged in tandem. Bulletin of the JSME 25, 349–357.

Igarashi, T., 1997. Drag reduction of a square prism by flow control using a small rod. Journal of Wind Engineering and Industrial Aerodynamics 69–71, 141–153.

Igarashi, T., Ito, S., 1993. Drag reduction of a square prism, 1st Report, Flow control around a square prism using a small vortex shedder. Transactions of JSME 59 (568), 3701–3707.

Igarashi, T., Tsutsui, T., 1989. Flow control around a circular cylinder by a new method, 1st Report, Forced reattachment of the separated shear layer. Transactions of JSME 55 (511), 701–706.

Klekar, K.M., Patankar, S.V., 1992. Numerical prediction of vortex shedding behind a square cylinder. International Journal for Numerical Methods in Fluids 14, 327–341.

Koenig, K., Roshko, A., 1985. An experimental study of geometrical effects on the drag and flow field of two bluff bodies separated by a gap. Journal of Fluid Mechanics 156, 167–204.

Lesage, F., Gartshore, I.S., 1987. A method of reducing drag and fluctuating side force on bluff bodies. Journal of Wind Engineering and Industrial Aerodynamics 25, 229–245.

Mahbub Alam, M.D., Moriya, M., Takai, K., Sakamoto, H., 2002. Suppression of fluid forces on two square prisms in a tandem arrangement by passive control of flow. Journal of Fluids and Structures 16, 1073–1092.

Morel, T., Bohn, M., 1980. Flow over two circular disks in tandem. ASME Journal of Fluids Engineering 102, 104–111.

Okajima, A., 1982. Strouhal number of rectangular cylinders. Journal of Fluid Mechanics 123, 379–398.

Sakamoto, H., Tan, K., Haniu, H., 1991. An optimum suppression of fluid forces by controlling a shear layer separated from a square prism. ASME Journal of Fluids Engineering 113 (2), 183–189.

Sohankar, A., Norberg, C., Davidson, L., 1996. A numerical study of unsteady two-dimensional flow around rectnagular cylinders at incidence. Internal Report No. 96/25, Department of Thermal and Fluid Dynamics, Chalmers University of Technology, Gothenburg, Sweden.

Sakamoto, H., Tan, K., Takeuchi, N., Haniu, H., 1997. Suppression of fluid forces acting on a square prism by passive control. ASME Journal of Fluids Engineering 119, 506–511.

Wolf-Gladrow, D.A., 2000. Lattice-Gas Cellular Automata and Lattice Boltzmann Models. Lecture Notes in Mathematics. Springer, Berlin.

Further reading

Davis, R.W., Moore, E.F., 1982. A numerical study of vortex shedding from rectangles. Journal of Fluid Mechanics 116, 475–506.